

First principles models of the interactions of methane and carbon dioxide

Mark T. Oakley, Hainam Do, Richard J. Wheatley*

School of Chemistry, University of Nottingham, University Park, Nottingham NG7 2RD, UK

ARTICLE INFO

Article history:

Received 31 July 2009

Received in revised form 5 November 2009

Accepted 9 November 2009

Available online 18 November 2009

Keywords:

Ab initio calculations

Potential energy surface

Gibbs ensemble

Vapor–liquid equilibrium

ABSTRACT

We present ab initio calculations on the CH₄–CH₄ and CH₄–CO₂ dimer potential energy surfaces. We show that the fit to these surfaces is improved over the Lennard–Jones potential by changing the form of the repulsive wall. Ab initio calculations are also performed on trimers to evaluate the strength of nonadditive interactions. The experimental CH₄ phase properties are reproduced in simulations that include correction for nonadditive dispersion. The phase-coexistence curve of mixtures of CH₄ and CO₂ is also improved by including this nonadditive dispersion term.

© 2009 Elsevier B.V. All rights reserved.

1. Introduction

A detailed understanding of the properties of mixtures of alkanes and CO₂ has a number of uses. The development of environmentally safe refrigerants is a great technical challenge and mixtures of CO₂ with hydrocarbons or hydrofluorocarbons are one possible solution. Supercritical CO₂ is also used in the extraction of oil. The simplest alkane is methane, and the mixture of CH₄ and CO₂ is a well-studied system, with its phase-coexistence behaviour measured over a range of temperatures and pressures [1,2]. With good experimental data available, and potential uses as an analogue for larger alkanes, the mixture of CH₄ and CO₂ is an excellent target for molecular simulations.

Intermolecular potentials are often fitted to reproduce the experimental properties of a system. Many potentials of this type are available for CO₂[3,4] and CH₄[5]. These potentials have also been used to model the vapor–liquid equilibria of mixtures of CO₂ and CH₄[4,6]. These empirical fits often perform well, but may be in error for properties or conditions they were not fitted to and cannot be applied to systems where no experimental data are available.

Potentials derived entirely from first-principles calculations can be used under any conditions. However, these potentials only perform well when the first-principles calculations explicitly include everything that could affect the simulated properties. Pair potentials fitted to ab initio calculations are available for CO₂[7–9] and CH₄[10]. Accurate pair potentials often perform poorly in modelling phase properties because of the lack of multi-body interactions

[11]. We have previously shown that an accurate pair potential and a correction for three-body dispersion reproduces the phase-coexistence line of CO₂[9].

We present ab initio calculations on the CH₄ dimer. The CH₄ molecule is nonpolar. Therefore, the interactions in the CH₄ dimer are dominated by dispersion forces, which can only be calculated with ab initio methods that have a good treatment of electron correlation. We show that the form of the repulsive wall has a substantial effect on the fit to the potential energy surface and on simulations using the resulting potentials. We also simulate mixtures of CH₄ and CO₂. In previous works, the parameters for CH₄/CO₂ interactions are obtained from mixing rules. Here, we construct a complete potential energy surface for the CH₄–CO₂ dimer and fit a potential to it. We also present ab initio calculations on trimers of CO₂ and CH₄ and use these to model the effect of nonadditive interactions in simulations.

2. Additive potentials

Potential energy surfaces are generated for the dimer of CH₄ and the dimer comprising one molecule of CH₄ and one of CO₂. The interaction energies of the dimers are evaluated using second order Møller–Plesset perturbation theory (MP2) in Molpro [12]. Counterpoise correction is used to correct the basis set superposition error. The geometries of the dimers are chosen with C–C or C–O distances between 5.0a₀ and 13.0a₀ in steps of 0.5a₀. The intermolecular angles are varied in steps of π/6 rad. Any geometries with H–H interactions closer than 2.5a₀ are excluded. This gives 9216 structures for CH₄–CH₄ and 12,791 for CH₄–CO₂. In all of these calculations, the geometries of the molecules are held rigid. Simulations of CO₂ with the EPM potential give similar phase-coexistence

* Corresponding author.

E-mail address: Richard.Wheatley@nottingham.ac.uk (R.J. Wheatley).

Table 1

The atomic charges and dipole moments of CH₄ (upper rows) and CO₂ (lower rows) calculated using iterated stockholder atoms with the MP2 method. In both molecules, the dipoles point outwards from the central C atoms.

Basis set	aug-cc-pVDZ	aug-cc-pVTZ	aug-cc-pVQZ
q_C	-0.393	-0.427	-0.434
q_H	0.098	0.107	0.108
μ_H	0.032	0.032	0.032
q_C	0.873	0.860	0.857
q_O	-0.436	-0.430	-0.428
μ_O	0.121	0.135	0.135

properties with rigid and flexible models [3]. Ab initio potentials using different C–O bond lengths to model vibrational averaging give phase-coexistence properties that are the same within the uncertainties of the simulations [9]. We assume that every molecule is in a single vibrational state and that mixing with higher energy states is small. Therefore, the influence of nuclear quantum effects on thermodynamics is ignored.

The energies of these structures are calculated with Dunning's aug-cc-pVDZ and aug-cc-pVTZ basis sets [13]. Calculations on ~10,000 structures of each dimer with larger basis sets are impractical. A subset of 1000 structures of each dimer is selected for MP2/aug-cc-pVQZ calculations. The structures are selected at random and accepted with a probability proportional to $1/(E + E')^2$, where E is the MP2/aug-cc-pVDZ dimer interaction energy and E' is $5m_e h$. This favours low energy structures, but also gives some coverage of the repulsive wall. Extrapolation to the complete basis set limit is performed for these 1000 geometries by an exponential fit to the double-, triple- and quadruple-zeta energies.

Potentials are fitted to these calculated energy surfaces. We also consider new forms of potential to fit to our 2414 point CO₂ dimer potential energy surface [9]. The potential for the interaction between two molecules, A and B , includes three terms: one to model electrostatic interactions, one for attractive induction/dispersion and one to model the repulsive wall

$$U_{AB} = U_{elec} + U_{attr} + U_{rep} \quad (1)$$

In our previous work, the electrostatic component of the potential comprised coulombic interactions between atomic point charges, with these charges fitted at the same time as the attractive and repulsive parts of the potential. Here, we take a different approach and take atomic charges and dipoles from iterated stockholder atom (ISA) calculations [14] on single CO₂ and CH₄ molecules. The charges and dipole moments are generated with the MP2 method using aug-cc-pVDZ, aug-cc-pVTZ and aug-cc-pVQZ basis sets (Table 1). The oxygen atoms on CO₂ are anisotropic and have

a substantial dipole moment. The electrostatic part of the potential includes charge–charge interactions for all pairs of atoms, with charge–dipole and dipole–dipole interactions where appropriate

$$U_{elec} = \sum_{a \in A} \sum_{b \in B} \left[\frac{q_a q_b}{r_{ab}} + \frac{q_a \mu_b \cdot R_{ab}}{r_{ab}^3} - \frac{3\mu_a \cdot R_{ab} \mu_b \cdot R_{ab}}{r_{ab}^5} + \frac{\mu_a \cdot \mu_b}{r_{ab}^3} \right] \quad (2)$$

where r_{ab} is the distance between atoms a and b , q are the atomic charges and μ are the atomic dipole moments.

The attractive dispersion term is proportional to r^{-6} :

$$U_{attr} = \sum_{a \in A} \sum_{b \in B} \left[\frac{C_{ab}^6}{r_{ab}^6} \right] \quad (3)$$

The repulsive part of the potential is more difficult to represent in a simple form. The Lennard–Jones potential, with the repulsion proportional to r^{-12} , is the most widely used because of its computational efficiency, but other potentials with exponential terms or several r^{-n} terms are more accurate. For example, Klein and Hanley's m-6-8 potential [15,16] performs well for several thermodynamic properties over a wide range of temperatures. Here, we find that the Lennard–Jones potential makes the repulsive wall too steep for H–H or heavy atom–H interactions. Replacing the r^{-12} with r^{-8} for these interactions significantly improves the fit to the potential energy surfaces. We have previously shown that the repulsive interactions in the CO₂ dimer are anisotropic and that this anisotropy is well represented by spherical tensors [9]:

$$U_{rep} = \sum_{a \in A} \sum_{b \in B} \left[\frac{C_{ab}^8}{r_{ab}^8} + \frac{C_{ab}^{12}}{r_{ab}^{12}} + \frac{C_{ab(011;00)}^{12} \mathbf{b} \cdot \hat{\mathbf{R}}}{r_{ab}^{12} \sqrt{3}} + \frac{C_{ab(101;00)}^{12} \mathbf{a} \cdot \hat{\mathbf{R}}}{r_{ab}^{12} \sqrt{3}} + \frac{C_{ab(110;00)}^{12} \mathbf{a} \cdot \mathbf{b}}{r_{ab}^{12} \sqrt{3}} + \frac{C_{ab(112;00)}^{12} (\mathbf{a} \cdot \mathbf{b} - 3 \times \mathbf{a} \cdot \hat{\mathbf{R}} \times \mathbf{b} \cdot \hat{\mathbf{R}})}{r_{ab}^{12} \sqrt{30}} \right] \quad (4)$$

Only one of the two isotropic terms is used for each pair of atoms, with r^{-8} used for any pairs involving a hydrogen atom and r^{-12} used for all other pairs. The first anisotropic term is used for any atom interacting with an oxygen atom in CO₂ and all four anisotropic terms are used for oxygen–oxygen interactions.

The parameters for the electrostatic component of the potential are obtained from single molecule ab initio calculations [14] and the C^6 , C^8 and C^{12} parameters for the dispersion and repulsion components are obtained by fitting to the MP2 potential energy surfaces. Potentials are fitted to the double- and triple-zeta potential energy surfaces by minimisation of the root mean square error, with a Boltzmann weighting scheme to improve the fit of the lowest

Table 2

Parameters in the CO₂ pair potentials. All quantities are in atomic units.

Potential	CBS-i	CBS-a	ISA-i	ISA-id	ISA-ad
q_C	0.559	0.534	0.857	0.857	0.857
q_O	-0.279	-0.267	-0.428	-0.428	-0.428
μ_O				0.135	0.135
C_{CC}^6	57.6	157	-340.0	-19.5	25.5
C_{CO}^6	-36.8	-95.2	124.7	-6.00	-40.8
C_{OO}^6	-31.8	1.14	-96.6	-44.0	-21.0
C_{CC}^{12}	3.51×10^5	1.65×10^5	3.26×10^6	7.39×10^5	6.32×10^5
C_{CO}^{12}	5.16×10^5	4.98×10^5	-4.73×10^5	4.11×10^5	3.71×10^5
C_{OO}^{12}	1.05×10^6	1.19×10^6	1.38×10^6	1.08×10^6	1.23×10^6
$C_{CO(011;00)}^{12}$		-8.70×10^5			-3.61×10^5
$C_{CO(011;00)}^{12}$		7.75×10^5			6.68×10^5
$C_{CO(101;00)}^{12}$		7.75×10^5			6.68×10^5
$C_{CO(110;00)}^{12}$		-4.13×10^4			2.09×10^4
$C_{CO(112;00)}^{12}$		-2.31×10^5			-1.28×10^5
$\sigma_{Boltz}/\mu E_h$	109	58	179	92	52

energy structures. A temperature of 1000 K is used for the Boltzmann weighting to provide good sampling of the repulsive wall. The parameters are generated by a linear least-squares fit and each set of parameters represents a unique best solution. However, the fitting surfaces are fairly flat, so many different sets of parameters can produce fits that are almost as good. The use of iterated stockholder atoms to generate the electrostatic parameters reduces the number of parameters that need to be fitted, which partially solves this problem.

Only 1000 points are available at the quadruple-zeta and complete basis set levels, which does not provide sufficient coverage of the potential energy surface for parameter fitting. However, the difference between the quadruple-zeta and triple-zeta energies varies more smoothly than the total energy and this is fitted as a difference potential. The parameters from this difference potential are then added to the triple-zeta parameters to obtain an effective quadruple-zeta potential. The same procedure is used to generate a complete basis potential.

The previously described parameters for CO₂ were fitted with a Boltzmann weighting at a temperature of 298 K. Here, we re-fit these parameters at 1000 K for consistency with the potentials for CH₄ and CH₄/CO₂ (Table 2). This leads to a small change in the fitted parameters, but the simulated physical properties remain within the standard errors of the previous simulations. We also consider three new potentials: ISA-i takes the same form as the CBS-i potential with the atomic charges taken from ISA calculations, ISA-id adds dipoles to the oxygen atoms and ISA-ad includes anisotropic r^{-12} terms in the repulsive wall. The ISA-i potential fits the MP2 surface poorly and produces unreasonable fitted parameters (such as the large negative C_{CO}^{12}). This is because the ISA charges, when taken alone, give a molecular quadrupole moment that is too large by a factor of about two. The inclusion of atomic dipoles in the ISA-id and ISA-ad potentials gives fitting errors that are slightly smaller than the CBS-i and CBS-a potentials.

The change from r^{-12} to r^{-8} for the repulsive interactions with hydrogen atoms significantly improves the fitting error in the CH₄ pair potential (Table 3). The use of atomic dipoles in CH₄ makes little difference to the parameter fit. This is because the CH₄ molecule does not have a dipole or quadrupole moment and the electrostatic term is much less important than it is in CO₂. The hydrogen atoms in CH₄ are relatively isotropic and the inclusion of anisotropic repulsive wall terms does not improve the fit. The addition of r^{-8} terms and atomic dipole moments improves the fit to the CH₄-CO₂ dimer

Table 3

Parameters in the CH₄ pair potentials calculated at the complete basis set limit. The Boltzmann-weighted RMS error, σ_{Boltz} , is calculated for 9216 point potential energy surface calculated at the MP2/aug-cc-pVDZ level. All quantities are in atomic units.

Potential	ISA-i	ISA-i8	ISA-id8
q_C	-0.434	-0.434	-0.434
q_H	0.108	0.108	0.180
μ_H			0.032
C_{CC}^6	-305	143	115
C_{CH}^6	0.410	-65.4	-68.4
C_{HH}^6	5.21	5.30	7.80
C_{CH}^8		1.21×10^3	1.27×10^3
C_{HH}^8		7.59×10^{-3}	-29.6
C_{CC}^{12}	1.32×10^7	2.06×10^6	1.80×10^6
C_{CH}^{12}	5.58×10^4		
C_{HH}^{12}	-5.88×10^{-2}		
$\sigma_{\text{Boltz}}/\mu E_h$	214	128	131

potential energy surface (Table 4). Taking account of the anisotropy of CO₂ in the CO and HO interactions also improves the fit.

3. Nonadditive potentials

To model the nonadditivity in the CH₄/CO₂ system, we need the nonadditive energies of four types of trimer: CH₄-CH₄-CH₄, CH₄-CH₄-CO₂, CH₄-CO₂-CO₂ and CO₂-CO₂-CO₂. For each type of trimer, 250 geometries are selected at random from Monte Carlo simulations. The trimers are chosen by selecting a molecule from a random timestep in a simulation, then selecting another with any atom within 4 Å of an atom in the first and finally selecting another molecule with an atom within 4 Å of either of the other two molecules. This selection procedure provides a range of geometries from equilateral triangular to linear. In mixed trimers, it returns linear geometries with ABB and BAB arrangements. Trimers of CH₄ are chosen from a simulation of the liquid phase at 100 K. Mixed trimers are chosen from a simulation of 50:50 mixture of CO₂ and CH₄ at 219 K. The previously described parameters for the CO₂ trimer are used without modification [9].

The nonadditive energy of a system is divided into three components: dispersion, induction and exchange-repulsion. These components are obtained from ab initio calculations on trimers. The nonadditive dispersion energy of each trimer is calculated using symmetry adapted perturbation theory (SAPT) at the RPA/aug-cc-pVTZ level, as described in our work on CO₂[9]. The sum of the

Table 4

Parameters in the CH₄-CO₂ pair potentials calculated at the complete basis set limit. The Boltzmann-weighted RMS error, σ_{Boltz} , is calculated for a 12,791 point potential energy surface calculated at the MP2/aug-cc-pVDZ level. The carbon atom in CO₂ is labelled as C'. All quantities are in atomic units.

Potential	ISA-i	ISA-i8	ISA-id8	ISA-ad8
q_C	-0.434	-0.434	-0.434	-0.434
q_H	0.108	0.108	0.108	0.108
$q_{C'}$	0.559	0.534	0.857	0.857
q_O	-0.279	-0.267	-0.428	-0.428
μ_H			0.032	0.032
μ_O			0.135	0.135
$C_{CC'}^6$	-112.0	-87.1	17.6	-7.2
C_{CO}^6	-131.7	-63.0	-103.7	-82.5
C_{HO}^6	11.1	1.07	-20.2	-17.0
$C_{CC'}^8$	12.0	-4.99	2.94	-1.44
C_{CO}^8		218	412	339
C_{HO}^8		250	186	268
$C_{CC'}^{12}$	2.09×10^6	1.53×10^6	9.90×10^5	8.48×10^5
C_{CO}^{12}	2.98×10^6	2.19×10^6	2.34×10^6	2.37×10^6
C_{HO}^{12}	1.15×10^4			
$C_{CC'}^{12}$	7.11×10^3			
$C_{CO(011;00)}^{12}$				-8.41×10^5
$C_{HO(011;00)}^{12}$				1.79×10^4
$\sigma_{\text{Boltz}}/\mu E_h$	194	161	157	136

Table 5Axilrod–Teller coefficients for CO₂, CH₄ and their mixed trimers. The carbon atom in CO₂ is labelled as C.

	CH ₄ –CH ₄ –CH ₄	CH ₄ –CH ₄ –CO ₂	CH ₄ –CO ₂ –CO ₂	CO ₂ –CO ₂ –CO ₂
	$\nu_{\text{CCC}} = 0.0$	$\nu_{\text{CCC}'} = 0.0$	$\nu_{\text{CC}'\text{C}'} = 0.0$	$\nu_{\text{C}'\text{C}'\text{C}'} = 0.4$
	$\nu_{\text{CCH}} = 0.0$	$\nu_{\text{CCO}} = 0.0$	$\nu_{\text{CC}'\text{O}} = 0.0$	$\nu_{\text{C}'\text{C}'\text{O}} = 3.2$
	$\nu_{\text{CHH}} = 0.0$	$\nu_{\text{CHC}'} = 0.0$	$\nu_{\text{COO}} = 0.0$	$\nu_{\text{C}'\text{O}\text{O}} = 25.9$
	$\nu_{\text{HHH}} = 20.4$	$\nu_{\text{CHO}} = 0.0$	$\nu_{\text{H}'\text{C}'\text{C}'} = 1.5$	$\nu_{\text{O}\text{O}\text{O}} = 209.0$
		$\nu_{\text{HHC}'} = 5.5$	$\nu_{\text{H}'\text{C}'\text{O}} = 11.9$	
		$\nu_{\text{HHO}} = 44.3$	$\nu_{\text{H}\text{O}\text{O}} = 96.2$	
RMS error/ μE_h	1.5	2.2	4.9	3.6

nonadditive induction and nonadditive exchange-repulsion energies is obtained from nonadditive MP2 calculations. These are calculated at the MP2/aug-cc-pVTZ level, with counterpoise correction to remove the basis set superposition error. We have shown that, in CO₂, the sum of the nonadditive MP2 and SAPT energies is close to the nonadditive CCSD(T) energy.

3.1. Nonadditive dispersion

The nonadditive dispersion energies of the pure CH₄ trimers are fitted to the Axilrod–Teller triple dipole dispersion energy [17]

$$U_{3,\text{disp}} = \frac{1}{6} \sum_{a,b,c} \nu_{abc} (1 + 3 \cos \theta_a \cos \theta_b \cos \theta_c) r_{ab}^{-3} r_{ac}^{-3} r_{bc}^{-3} \quad (5)$$

where r_{ab} is the distance between atoms a and b and θ_a is the angle at a made by atoms b , a and c (where a , b and c are all in different molecules). The Axilrod–Teller coefficients, ν , of CH₄ are fitted to the calculated nonadditive dispersion energies by minimisation of the unweighted root mean square error. The nonadditive dispersion energies of the CH₄ trimer fall between $-5 \mu\text{E}_h$ and $70 \mu\text{E}_h$. This is a similar range to the nonadditive dispersion energies seen in CO₂ [9]. The nonadditive dispersion of CH₄ is fitted to the Axilrod–Teller equation (5) with an RMS error of $1.6 \mu\text{E}_h$ (Table 5). The calculated total Axilrod–Teller coefficient of CH₄ is 1303 a.u., which is in good agreement with the experimental value of 1630 a.u. [18].

Faster calculation of the nonadditive dispersion energies in a simulation could be achieved with a united atom representation of CH₄. If Axilrod–Teller coefficients are fitted only to the carbon atoms, the nonadditive dispersion energies are reproduced with an RMS error of $3.0 \mu\text{E}_h$. This gives $\nu_{\text{CCC}} = 2447$, which is significantly further from the experimental value.

The Axilrod–Teller coefficients of the mixed trimers are not fitted to the SAPT energies of the mixed trimers, but are generated in geometric progressions from these CH₄ parameters and our previously generated CO₂ parameters [9]. These parameters reproduce the nonadditive dispersion energies of CH₄–CH₄–CO₂ and CH₄–CO₂–CO₂ with RMS errors of 2.2 and $4.9 \mu\text{E}_h$ respectively. This transferability of Axilrod–Teller coefficients will be useful when developing new potentials for other molecules.

3.2. Nonadditive induction

The nonadditive induction energies are represented by

$$U_{3,\text{ind}} = \frac{1}{2} \sum_{a,b,c} -q_a q_c \alpha_b r_{ab}^{-2} r_{bc}^{-2} \cos \theta_b \quad (6)$$

with the atomic charges, q , on CH₄ taken from iterated stockholder atoms [14] and the atomic charges on CO₂ fitted to reproduce the quadrupole moment [9]. The atomic polarisabilities, α , are calculated at the MP2/aug-cc-pVTZ level [19]. The atomic polarisabilities in CO₂ are 7.706 a.u. for carbon and 8.039 a.u. for oxygen. A united atom representation is used for CH₄, with the molecular polarisability at 15.968 a.u..

In CH₄–CO₂–CO₂, the nonadditive MP2 energy varies from $-90 \mu\text{E}_h$ to $45 \mu\text{E}_h$. The nonadditive induction energy calculated with (6) reproduces this with an RMS error of $9.4 \mu\text{E}_h$. In CH₄–CH₄–CH₄ and CH₄–CH₄–CO₂, the nonadditive induction energies calculated with (6) are small ($< 1 \mu\text{E}_h$) because the nonpolar CH₄ molecules only cause very small induced dipoles. In both of these cases, the nonadditive MP2 energy is almost entirely due to exchange-repulsion.

3.3. Nonadditive exchange-repulsion

Any nonadditive energy not fitted by Eqs. (5) and (6) is taken to be exchange-repulsion. In the CO₂ trimer, the exchange-repulsion is difficult to interpret in terms of interatomic interactions because the nonadditive exchange-repulsion energy includes the fitting errors in the induction and dispersion. In the CH₄ trimer, the nonadditive MP2 energy is mostly exchange-repulsion. Analysis of the C–C–C angles (Fig. 1) and distances (Fig. 2) reveals a set of 12 structures with substantial negative exchange-repulsion energies. All of these trimers have the three molecules in an equilateral triangle with the centres of the molecules within $8a_0$ of each other.

We fit the nonadditive exchange-repulsion energies with

$$U_{3,\text{exch}} = \sum_{a,b,c} A_{abc} r_{ab}^{-6} r_{bc}^{-6} r_{ac}^{-6} + B_{abc} r_{ab}^{-6} r_{bc}^{-6} \cos \theta_b \quad (7)$$

A two parameter fit, with $A_{\text{HHH}} = -3.6 \times 10^6$ a.u. and $B_{\text{HHH}} = -13 \times 10^3$ a.u. performs well, with an RMS error of $1.9 \mu\text{E}_h$. Including parameters for the CC and CH interactions only improves the RMS error to $1.7 \mu\text{E}_h$.

4. Molecular simulations

All terms in the energy are calculated up to a cut-off distance of 12 Å. If this cut-off is applied to interatomic distances, the electrostatic energies of molecules that are partially outside the cut-off will

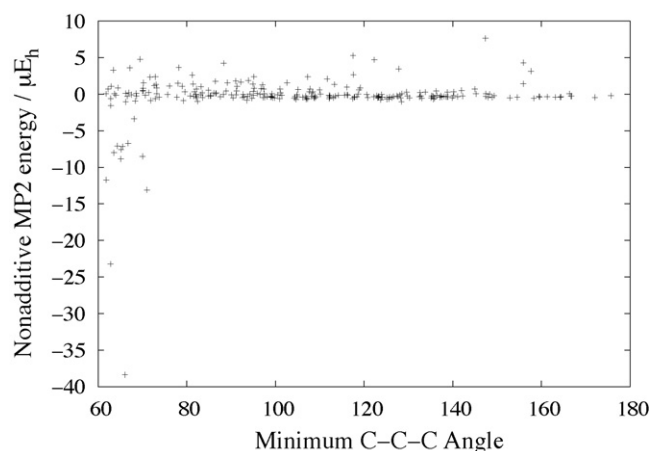


Fig. 1. Angle dependence of the nonadditive MP2 energy in the CH₄ trimer.

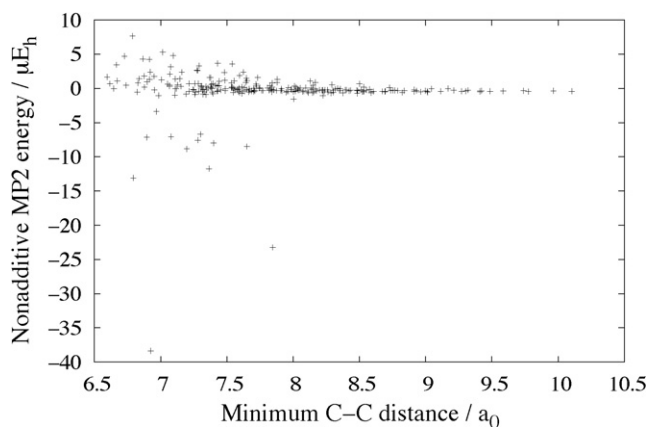


Fig. 2. Distance dependence of the nonadditive MP2 energy in the CH₄ trimer.

be incorrect. Therefore, the cut-off is applied to whole molecules, with the distance measured from the central carbon atom in each molecule. A long-range correction with the form

$$U_{\text{long-range}} = \frac{4}{3} \pi \rho B r_{\text{cut}}^{-3} \quad (8)$$

is applied to account for the truncation of the r^{-6} term.

The phase-coexistence properties are simulated using NVT Gibbs ensemble Monte Carlo [20]. In this ensemble, the liquid and gas phases are simulated simultaneously using periodic boundary conditions. The Monte Carlo moves include translations and rotations of a single molecule within a phase. Additionally, a molecule can move from one phase to the other or the volumes of the two phases can change to equalise the pressure and chemical potential of the two phases. Any increase in the volume of one phase is accompanied by an equal decrease in the volume of the other phase to maintain the constant volume condition.

Simulations are performed on 400 molecules, with the volume chosen to give approximately 200 molecules in each phase. Each simulation comprises 100,000 passes, with the first 10,000 used for equilibration. At each step, the molecule and type of move is chosen at random. Each Monte Carlo pass includes, on average, one attempted translation or rotation per molecule, 100 swap moves and one volume move.

The critical temperatures of the single-component systems are determined from a fit to the scaling law,

$$(\rho_l - \rho_g) = A(T_c - T)^\beta \quad (9)$$

where β is the critical exponent and A is a proportionality constant. The critical densities are obtained from fits to the law of rectilinear diameters,

$$\frac{1}{2}(\rho_l + \rho_g) = \rho_c + A(T - T_c) \quad (10)$$

Table 7

The phase properties of CO₂ calculated with two effective nonadditive potentials. Values in parentheses are the uncertainties at the 95% confidence level. Experimental data from NIST WebBook [22].

	Experiment	EPM	CBS-a	ISA-ad
$\Delta H_{\text{vap}}^{228} / \text{kJ mol}^{-1}$	14.49	15.07 (0.03)	15.23 (0.03)	15.32 (0.09)
$\Delta H_{\text{vap}}^{288} / \text{kJ mol}^{-1}$	7.81	9.50 (0.06)	9.12 (0.06)	9.77 (0.21)
$\rho_l^{228} / \text{kg m}^{-3}$	1134.9	1106 (2)	1150 (2)	1143 (5)
$\rho_l^{288} / \text{kg m}^{-3}$	824.4	850.6 (4)	810.1 (18.6)	804.4 (26.4)
$\rho_g^{228} / \text{kg m}^{-3}$	21.8	19.3 (1.2)	16.8 (0.4)	14.5 (1.0)
$\rho_g^{288} / \text{kg m}^{-3}$	160.7	123.2 (3)	111.3 (3.2)	85.5 (5.5)
P_{228} / bar	8.2	7.6 (0.3)	6.5 (0.1)	5.6 (0.4)
P_{288} / bar	50.2	45.0 (1.1)	37.9 (0.7)	34.0 (1.5)
T_c / K	304	313	305	310
$\rho_c / \text{kg m}^{-3}$	466.4	453.7	431.1	411.2

Table 6

Calibration of the density-dependent nonadditive term in mixtures of CH₄ and CO₂.

CH ₄ mole fraction	0%	25%	50%	75%	100%
k	9.70	8.74	7.90	6.91	6.24

In CO₂, the nonadditive dispersion energy adds a significant repulsive interaction when the energy of a whole box is calculated. However, the contributions from nonadditive induction and nonadditive exchange-repulsion are small. The explicit calculation of nonadditive dispersion energies is extremely expensive. We have shown the nonadditive dispersion energy of CO₂ is correlated with its density, and that a density-dependent potential significantly improves the simulated phase properties. We fit a similar density-dependent potential for CH₄:

$$U_{\text{nonadd}} = k\rho^{2.5} \quad (11)$$

where U_{nonadd} is the nonadditive energy per molecule and ρ is the number density of the phase and k is a fitted constant. The density-dependent term in mixtures of CH₄ and CO₂ takes the same form, with k scaled according to the mole fraction of the components. The validity of this approximation is checked with single-phase NVT Monte Carlo simulations. These simulations are performed on mixtures with 25%, 50% and 75% CH₄, at temperatures of 180 K and 230 K, and at pressures from 20 to 80 bar. Density-dependent potentials are fitted to each set of calculations and the fitted parameter varies smoothly with the mole fraction in the simulation (Table 6).

In our previous work [9], we showed that ab initio potentials with the same form as the EPM potential lead to over-binding in the liquid phase of CO₂. The inclusion of anisotropic interactions in the CBS-a potential and nonadditive dispersion gives phase-coexistence properties that are in good agreement with those from the empirical EPM2 potential [3] and the experimental results. Gibbs ensemble simulations with the new ISA-id and ISA-ad CO₂ potentials lead to properties that are, within the uncertainties of the simulation, the same as those produced with the CBS-a potential (Table 7).

The potentials described here are more complicated than the EPM2 potential. The addition of the density-dependent nonadditive term (11) leads to a negligible increase in the required computational resources. The anisotropic terms in the CBS-a and ISA-id increase the length of the simulations by a factor of about 2. Including both sets of anisotropic parameters in the ISA-ad potential leads to a 3-fold increase in the required time, but gives no further improvement in the calculated phase-coexistence properties. The CBS-a and ISA-id potentials represent the best compromise between accuracy and computational expense.

As the size of the basis set increases, the strength of the CH₄ binding increases (Table 8), leading to larger enthalpies of vaporisation, higher liquid densities, lower gas densities and lower pressures. However, even at the complete basis set limit, a charge

Table 8

The phase properties of CH₄ calculated with ISI-i8 pair potentials with various basis sets. Values in parentheses are the uncertainties at the 95% confidence level. Experimental data from NIST WebBook [22].

	Experiment	aug-cc-pVDZ	aug-cc-pVTZ	aug-cc-pVQZ	CBS
$\Delta H_{\text{vap}}^{100} / \text{kJ mol}^{-1}$	8.52	7.30 (0.01)	8.61 (0.03)	9.37 (0.03)	9.62 (0.03)
$\Delta H_{\text{vap}}^{180} / \text{kJ mol}^{-1}$	3.95	n/a	5.29 (0.04)	6.22 (0.04)	6.58 (0.04)
$\rho_l^{100} / \text{kg m}^{-3}$	438.6	389.7 (0.5)	430.5 (1.0)	452.6 (0.5)	459.2 (0.5)
$\rho_l^{180} / \text{kg m}^{-3}$	275.9	n/a	302.2 (1.3)	324.6 (2.4)	335.0 (1.6)
$\rho_g^{100} / \text{kg m}^{-3}$	0.7	1.5 (0.1)	0.5 (0.0)	0.4 (0.0)	0.3 (0.0)
$\rho_g^{180} / \text{kg m}^{-3}$	61.6	n/a	38.8 (0.9)	29.3 (1.3)	26.1 (1.1)
P_{100} / bar	0.4	0.8 (0.0)	0.3 (0.0)	0.2 (0.0)	0.2 (0.0)
P_{180} / bar	32.9	n/a	23.7 (0.3)	20.7 (0.6)	19.0 (0.6)

Table 9

The phase properties of CH₄ calculated with pair and nonadditive potentials. Values in parentheses are the uncertainties at the 95% confidence level. Experimental data from NIST WebBook [22].

	Experiment	TraPPE-EH	Additive ISA-i	Additive ISA-i8	Nonadditive ISI-i8
$\Delta H_{\text{vap}}^{100} / \text{kJ mol}^{-1}$	8.52	8.73 (0.02)	6.87 (0.01)	9.62 (0.03)	8.55 (0.01)
$\Delta H_{\text{vap}}^{180} / \text{kJ mol}^{-1}$	3.95	3.92 (0.06)	n/a	6.58 (0.04)	5.02 (0.04)
$\rho_l^{100} / \text{kg m}^{-3}$	438.6	443.4 (0.8)	413.0 (1.5)	459.2 (0.8)	426.6 (0.9)
$\rho_l^{180} / \text{kg m}^{-3}$	275.9	267.1 (8.3)	n/a	335.0 (1.6)	280.6 (3.3)
$\rho_g^{100} / \text{kg m}^{-3}$	0.7	0.6 (0.0)	2.8 (0.1)	0.3 (0.0)	0.5 (0.0)
$\rho_g^{180} / \text{kg m}^{-3}$	61.6	62.7 (4.3)	n/a	26.1 (1.1)	37.4 (1.4)
P_{100} / bar	0.4	0.3 (0.0)	1.4 (0.0)	0.2 (0.0)	0.3 (0.0)
P_{180} / bar	32.9	35.2 (1.2)	n/a	19.0 (0.6)	24.0 (0.5)
T_c / K	191	190	163	214	199
$\rho_c / \text{kg m}^{-3}$	162.0	161	161.3	159.2	146.2

plus Lennard–Jones potential gives enthalpies of vaporisation that are too low (Table 9). The inclusion of an r^{-8} repulsion term leads to stronger CH₄ binding, giving a system that is too strongly bound. The addition of a density-dependent nonadditive term (11) adds a substantial repulsive interaction, which gives phase-coexistence properties closer to the experimental values (Fig. 3). The liquid line on the phase-coexistence curve calculated with the ISA-i8 potential is in good agreement with the experimental data and the line calculated with the TraPPE-EH potential [5]. However, our simulations underestimate the density of the gas phase. This leads to a higher critical pressure and lower critical density for CH₄.

Mixtures of CO₂ and CH₄ are simulated with the NPT Gibbs ensemble [21]. Simulations with the ISA-i8 and ISA-id8 potentials give phase-coexistence curves that are the same to within the uncertainties of the simulations. Here, we only present the results with the ISA-i8 potential. The ab initio pair potentials perform well in reproducing the liquid part of the phase-coexistence curve of a CH₄/CO₂ mixture, but give too much CH₄ in the gas phase (Fig. 4). Nonadditive dispersion destabilises the CO₂-rich liquid and forces

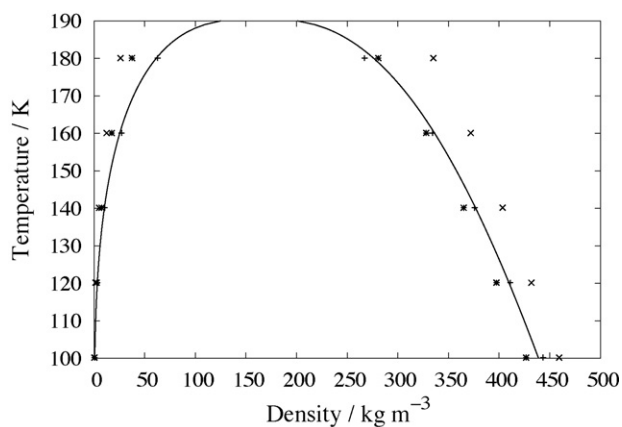


Fig. 3. Liquid–vapor coexistence densities of CH₄ from experiment [22] (solid line) and calculated using the TraPPE-EH (+) additive ISA-i8 (×) and nonadditive ISA-i8 (*) potentials.

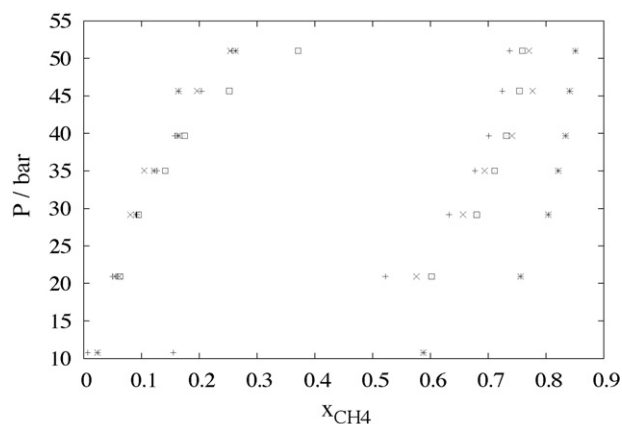


Fig. 4. The phase-coexistence curve of CH₄/CO₂ at 230 K from experiment [2] (+) and calculated using the TraPPE-EH (×), additive ISA-i8 (*) and nonadditive ISA-i8 (□) potentials.

some of it into the gas phase, which decreases the mole fraction of CH₄ and places it in better agreement with the experimental curve. The composition of the gas phase calculated with the nonadditive ISA-i8 potential is close to that calculated with the empirical TraPPE-EH potential [4,5]. At low pressures, the nonadditive term does not change the composition of the liquid phase. At higher pressures the amount of CH₄ in the liquid phase is overestimated. It is possible that the effective nonadditive term is the cause of this error as the parameter k is fitted to other fitted parameters. Calculations with an explicit treatment of the nonadditive energy need to be performed to resolve this.

5. Conclusions

Fitted potentials containing atomic charges and dipoles from the iterated stockholder atoms method perform well in fitting the potential energy surfaces for dimers. The inclusion of atomic dipoles is important for CO₂, which has a high degree of atomic anisotropy.

The methods for fitting pair and three-body potentials that we developed for CO₂ perform just as well for the systems described here. The phase properties of CH₄ and CH₄/CO₂ calculated with effective nonadditive potentials are close to the experimental values. However, the agreement with experiment is not as good for these systems as it is for CO₂.

The Axilrod–Teller coefficients fitted to single-component trimers are transferable, and reproduce the nonadditive dispersion energies of mixed trimers well, which is will be a useful feature when developing potentials for other molecules.

Acknowledgements

We thank Professor Jonathan Hirst for helpful discussions. We thank the University of Nottingham High-Performance Computing facility for providing the computer resources used in this study and the Engineering and Physical Sciences Research Council for funding (grant number EP/E06082X/1).

References

- [1] S.C. Mraw, S.C. Hwang, R. Kobayashi, *J. Chem. Eng. Data* 23 (2) (1978) 135–139.
- [2] M.S.W. Wei, T.S. Brown, A.J. Kidnay, E.D. Sloan, *J. Chem. Eng. Data* 40 (4) (1995) 726–731.
- [3] J.G. Harris, K.H. Yung, *J. Phys. Chem.* 99 (31) (1995) 12021–12024.
- [4] J.J. Potoff, J.I. Siepmann, *AIChE J.* 47 (7) (2001) 1676–1682.
- [5] B. Chen, J.I. Siepmann, *J. Phys. Chem. B* 103 (25) (1999) 5370–5379.
- [6] G. Kamath, J.J. Potoff, *Fluid Phase Equilib.* 246 (1–2) (2006) 71–78.
- [7] S. Bock, E. Bich, E. Vogel, *Chem. Phys.* 257 (2–3) (2000) 147–156.
- [8] R. Bukowski, J. Sadlej, B. Jeziorski, P. Jankowski, K. Szalewicz, *J. Chem. Phys.* 110 (8) (1999) 3785–3803.
- [9] M.T. Oakley, R.J. Wheatley, *J. Chem. Phys.* (2009) 034110.
- [10] S.-W. Chao, A.H.-T. Li, S.D. Chao, *J. Comp. Chem.* 30 (2009) 1839–1849.
- [11] M.J. Elrod, R.J. Saykally, *Chem. Rev.* 94 (7) (1994) 1975–1997.
- [12] H.-J. Werner, P.J. Knowles, R. Lindh, F.R. Manby, M. Schütz, P. Celani, T. Korona, G. Rauhut, R.D. Amos, A. Bernhardsson, D.L. Berning, M.J.O. Cooper, A.J. Deegan, F. Dobbyn, C. Eckert, G. Hampel, A.W. Hetzer, S.J. Lloyd, W. McNicholas, M.E. Meyer, A. Mura, P. Nicklass, R. Palmieri, U. Pitzer, H. Schumann, A.J. Stoll, R. Stone, T. Tarroni, Thorsteinsson, MOLPRO, Version 2006.1, A Package of Ab Initio Programs, 2006.
- [13] R.A. Kendall, T.H. Dunning, R.J. Harrison, *J. Chem. Phys.* 96 (9) (1992) 6796–6806.
- [14] T.C. Lillistolen, R.J. Wheatley, *Chem. Commun.* (45) (2008) 5909–5911.
- [15] M. Klein, H.J.M. Hanley, *J. Chem. Phys.* 53 (12) (1970) 4722–4723.
- [16] H.J.M. Hanley, M. Klein, *J. Phys. Chem.* 76 (12) (1972) 1743–1751.
- [17] B.M. Axilrod, E. Teller, *J. Chem. Phys.* 11 (6) (1943) 299–300.
- [18] M.H. Champagne, X. Li, K.L.C. Hunt, *J. Chem. Phys.* 112 (4) (2000) 1893–1906.
- [19] T.C. Lillistolen, R.J. Wheatley, *J. Phys. Chem. A* 111 (2007) 11141–11146.
- [20] A.Z. Panagiotopoulos, *Mol. Phys.* 61 (4) (1987) 813–826.
- [21] A.Z. Panagiotopoulos, N. Quirke, M. Stapleton, D.J. Tildesley, *Mol. Phys.* 63 (4) (1988) 527–545.
- [22] E.W. Lemmon, M.O. McLinden, D.G. Friend, in: P.J. Linstrom, W.G. Mallard (Eds.), *Thermophysical Properties of Fluid Systems in NIST Chemistry WebBook*, NIST Standard Reference Database Number 69, National Institute of Standards and Technology, Gaithersburg, MD 20899, <http://webbook.nist.gov> (retrieved July 7, 2009).